

Magnetization, Magnetic Susceptibility and ESR in $\text{Tb}_3\text{Ga}_5\text{O}_{12}$

U. Löw,¹ S.A. Zvyagin,² M. Ozerov,² U. Schaufuss,³ V. Kataev,³ B. Wolf,⁴ and B. Lüthi⁴

¹*Theoretische Physik II, Technische Universität Dortmund, 44227 Dortmund, Germany*

²*Dresden High Magnetic Field Laboratory (HLD),*

Helmholtz-Zentrum Dresden-Rossendorf (HZDR), 01314 Dresden, Germany

³*Leibniz Institute for Solid State and Materials*

Research IFW Dresden, D-01171 Dresden, Germany

⁴*Physikalisches Institut, Universität Frankfurt,*

Max-von-Laue Strasse 1, 60438 Frankfurt, Germany

Abstract

We report on the measurement of the magnetic susceptibility and of ESR transitions in the garnet substance $\text{Tb}_3\text{Ga}_5\text{O}_{12}$ (TGG). The results are compared with a calculation in the framework of crystal field theory for the orthorhombic surroundings of the six inequivalent Tb ions of TGG. We also present a calculation of the magnetization for the three main crystal directions.

PACS numbers: 71.70.Ch, 75.30.Sg, 76.30.-v

I. INTRODUCTION

$\text{Tb}_3\text{Ga}_5\text{O}_{12}$ (TGG) is a dielectric material with a cubic garnet structure. Each Tb^{3+} ion has the same D_2 symmetry in its own local coordinate system which leads to pronounced crystal field (CEF) effects in various physical properties. TGG exhibits a transition to a antiferromagnetically ordered phase at 0.35K (ref.[1, 2]). The terbium ions are located on inter-penetrating triangular lattices, but they do not form a simple Kagome lattice, where the triangles lie in a plane, but are arrayed in three dimensions, forming a so-called Hyperkagome lattice [3], which like the Kagome lattice is geometrically frustrated.

Various interesting experiments have been performed recently with this substance. One of them is the phonon Hall effect. In analogy to the classical Hall effect in conducting materials, the appearance of a thermal gradient in the direction perpendicular to both, the applied magnetic field and the thermal flux, was observed [4, 5]. Another experiment is the acoustic Faraday effect where the rotation of a linearly polarized ultrasonic wave in a magnetic field applied along the propagation direction was observed and quantitatively analyzed [6, 7]. In another experiment the temperature dependence of the symmetry elastic constants were measured and interpreted with a simple CEF-model [8].

The aim of this paper is to show, that a CEF-Hamiltonian for the orthorhombic surroundings of the Tb ions is well fitted to describe the low energy spectrum and the thermodynamic properties of TGG. We expect that this is also of interest for a detailed model of transport phenomena like the phonon Hall effect.

First we discuss the CEF-Hamiltonian, next we calculate the magnetization in the three important crystal directions in high magnetic field and compare the result with existing experiments [9]. Afterwards we show experimental results of the magnetic susceptibility and compare it with analogous calculations. Finally we discuss our ESR results and interpret them using the same CEF-model.

II. CEF-MODEL

A Tb^{3+} ion has 8 4f-electrons leading with Hunds rule to $S=3$, $L=3$ and $J=6$. The CEF for these ions with local orthorhombic symmetry can be described with a Hamiltonian, introduced by Guillot et al. [9] in 1985, which in our notation reads:

b_{20}	b_{22}	b_{40}	b_{42}	b_{44}	b_{60}	b_{62}	b_{64}	b_{66}
-81.0	169.0	-2163.0	249.0	945.0	677.0	-155.0	1045.0	-4.0

TABLE I: Crystal field parameters b_{ij} for TGG in cm^{-1} as given in ref.[9]

$$\begin{aligned} \mathcal{H}_{loc} = & B_{20}\mathcal{O}_{20} + B_{22}\mathcal{O}_{22} + B_{40}\mathcal{O}_{40} + B_{42}\mathcal{O}_{42} + B_{44}\mathcal{O}_{44} \\ & + B_{60}\mathcal{O}_{60} + B_{62}\mathcal{O}_{62} + B_{64}\mathcal{O}_{64} + B_{66}\mathcal{O}_{66} + g\mu_B\vec{B}\vec{J}. \end{aligned} \quad (1)$$

Here \vec{B} is the magnetic field in the local coordinate system of a Tb^{3+} ion. The \mathcal{O}_{ij} are the Stevens operators as defined in [10], and the B_{ij} are the crystal field parameters. The B_{ij} can be calculated from the b_{ij} given in ref. [9]. We list the b_{ij} from [9] in table I and give the explicit relation between the b_{ij} and the B_{ij} in the appendix. For a detailed discussion of the conventions used in defining the crystal field parameters see e.g.[11].

In this paper we use the Hamiltonian given by eq.1 and take into account the six inequivalent ions in the unit cell [12] to calculate the magnetization, the susceptibility and ESR matrix elements of TGG. The local axis of the coordinate systems and the rotation matrices connecting the local and laboratory coordinate systems are given in table II.

Diagonalization of the Hamiltonian eq.1 gives the energy levels for the six ions as a function of magnetic field. These are given in fig.1. For $B=0$ we find a low lying quasi doublet, 3.7K apart, followed by a quasi triplet, with energy levels between 60K and 64K and a singlet at 67.8K. All other remaining singlets are above 433K. For cubic symmetry we would have a ground state doublet and an excited triplet followed by a singlet. The splitting from cubic to orthorhombic symmetry is therefore small.

In finite magnetic fields we observe crossovers of the energy levels. As field direction we take the three experimentally most common cases, the magnetic field parallel to the cubic $[110]_c$ direction (see ref. [9]), parallel to cubic $[100]_c$ direction (see ref.[6, 7]) and parallel to cubic $[111]_c$ direction, corresponding to the main axis of the crystal. The most interesting crossovers occur for the lowest energy levels in fig.1a at 9T for $B \parallel [110]_c$, in fig.1e at 20T for $B \parallel (100)$ and in fig.1f at 27T for $B \parallel [111]_c$.

Rotation Matrix	$(e_x)_{local}$	$(e_y)_{local}$	$(e_z)_{local}$
$R^1 = \begin{pmatrix} 0 & \frac{1}{\sqrt{2}} & \frac{1}{\sqrt{2}} \\ 0 & -\frac{1}{\sqrt{2}} & \frac{1}{\sqrt{2}} \\ 1 & 0 & 0 \end{pmatrix}$	$[001]_c$	$[1\bar{1}0]_c$	$[110]_c$
$R^2 = \begin{pmatrix} 0 & -\frac{1}{\sqrt{2}} & \frac{1}{\sqrt{2}} \\ 1 & 0 & 0 \\ 0 & \frac{1}{\sqrt{2}} & \frac{1}{\sqrt{2}} \end{pmatrix}$	$[010]_c$	$[\bar{1}01]_c$	$[101]_c$
$R^3 = \begin{pmatrix} 1 & 0 & 0 \\ 0 & \frac{1}{\sqrt{2}} & \frac{1}{\sqrt{2}} \\ 0 & -\frac{1}{\sqrt{2}} & \frac{1}{\sqrt{2}} \end{pmatrix}$	$[100]_c$	$[01\bar{1}]_c$	$[011]_c$
$R^4 = \begin{pmatrix} 0 & \frac{1}{\sqrt{2}} & -\frac{1}{\sqrt{2}} \\ 0 & \frac{1}{\sqrt{2}} & \frac{1}{\sqrt{2}} \\ 1 & 0 & 0 \end{pmatrix}$	$[001]_c$	$[110]_c$	$[\bar{1}10]_c$
$R^5 = \begin{pmatrix} 0 & \frac{1}{\sqrt{2}} & \frac{1}{\sqrt{2}} \\ 1 & 0 & 0 \\ 0 & \frac{1}{\sqrt{2}} & -\frac{1}{\sqrt{2}} \end{pmatrix}$	$[010]_c$	$[101]_c$	$[10\bar{1}]_c$
$R^6 = \begin{pmatrix} 1 & 0 & 0 \\ 0 & \frac{1}{\sqrt{2}} & -\frac{1}{\sqrt{2}} \\ 0 & \frac{1}{\sqrt{2}} & \frac{1}{\sqrt{2}} \end{pmatrix}$	$[100]_c$	$[011]_c$	$[0\bar{1}1]_c$

TABLE II: Rotation matrices from the local coordinate systems of the six inequivalent Tb ions to the laboratory system (column 1). Axis of the local coordinate systems of the six ions (column 2,3,4).

III. MAGNETIZATION

Since the energy levels of TGG display a complex structure of level crossings it is worthwhile to consider the magnetization, though due to the strong magneto-caloric effect [7], the magnetization of TGG in pulsed high fields is difficult to measure. We calculate

$$\langle J_k^i \rangle = -\frac{1}{Z} Tr \{ J_k \exp(-\beta(\mathcal{H}^i + g\mu_B \vec{B} \vec{J})) \} \quad (2)$$

where $\langle J_k^i \rangle$ is the contribution of the i th ion to the k th component ($k = x, y, z$) of

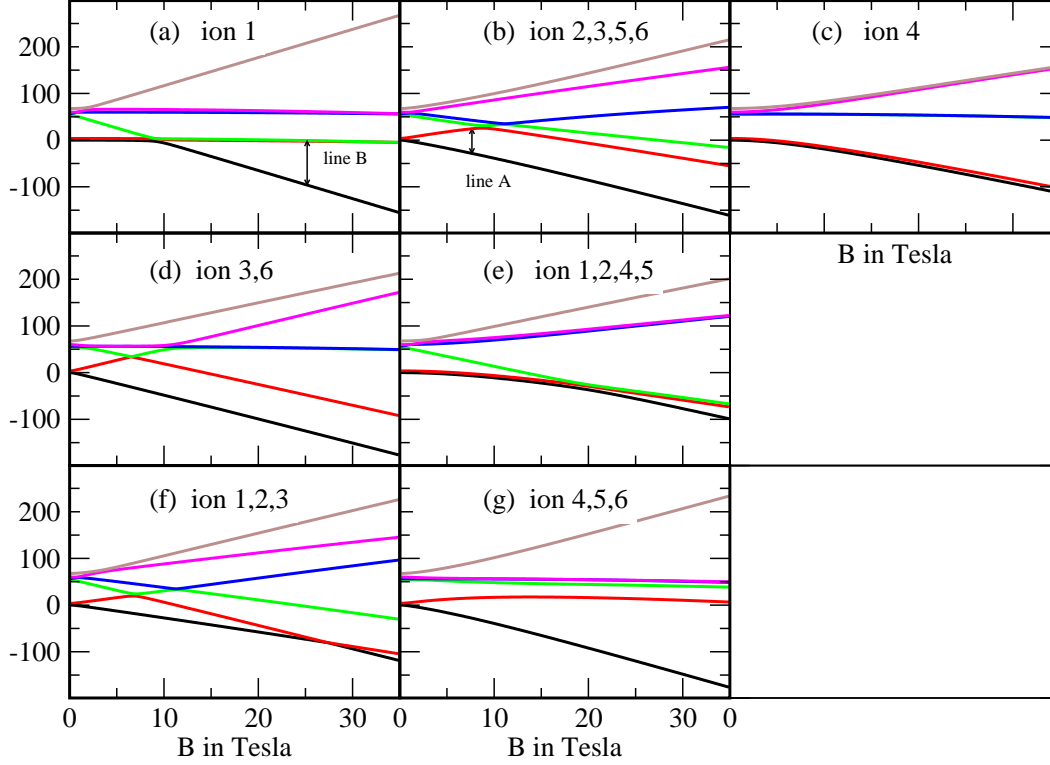


FIG. 1: Figure a,b,c show the six lowest energy levels for field in $[110]_c$ direction, figure d,e are the corresponding levels for field in $[100]_c$ direction, and figure f,g for field in $[111]_c$ direction. The corresponding ions are marked in the figures, the energies are in Kelvin and the magnetic field is in Tesla.

the magnetization in the laboratory system. The components of the total magnetization vector are given by $\langle J_k \rangle = \sum_{i=1}^6 \langle J_k^i \rangle$. Z is the partition function. Note that the \mathcal{H}^i are the Hamiltonians in the laboratory system and also \vec{B} is now the magnetic field in the laboratory system. We obtained the \mathcal{H}^i by a rotation of \mathcal{H}_{loc} from the local systems l_i [13][14]. Equivalently one can of course calculate the magnetizations in the local systems and transform them back to the laboratory system, which for a simple vector quantity like the magnetization would be definitely the method of choice. However in view of a more complex study in future concerning the elastic constants of TGG in high magnetic field we choose to rotate the Hamiltonians. This means that the \mathcal{H}^i we are dealing with in our calculations are more complex than the Hamiltonian given in eq.1, since e.g., also \mathcal{O}_{ij} with j odd appear. The crystal field constants in the laboratory system were calculated by Mathematica. Once these rotations are done the calculation of the observables discussed

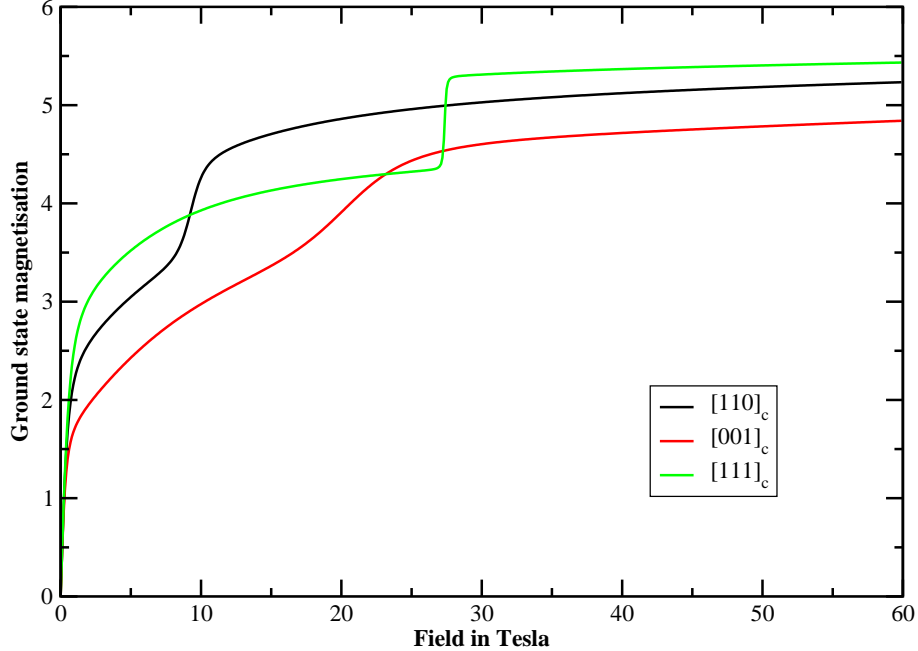


FIG. 2: Ground state magnetization $|\langle \vec{J} \rangle| = (\langle J_x \rangle^2 + \langle J_y \rangle^2 + \langle J_z \rangle^2)^{1/2}$ with the field parallel to the $[110]_c$, $[001]_c$, $[111]_c$. The saturation is at $|\langle \vec{J} \rangle| = 6$.

in this paper can all be conveniently performed in the laboratory system.

Fig.2 shows the total magnetization $|\langle \vec{J} \rangle| = (\langle J_x \rangle^2 + \langle J_y \rangle^2 + \langle J_z \rangle^2)^{1/2}$ at $T=0$ for the three field directions. The steps and plateaux in the magnetization mark cross-overs of the lowest levels as pointed out above. Changes of slope also occur because of the summation of the contributions of the different ions. So far only the magnetization in $[110]_c$ direction was measured and calculated. For this direction our results agree with Guillot et al. [9]. We want to point out, that the magnetizations in the other directions also exhibit interesting cross-over phenomena, which could be used to corroborate the validity of the underlying CEF-model up to high fields. Crossover effects at 20T for $B \parallel [100]_c$ have been observed previously in acoustic measurements [7].

Since in ref.[9] the magnetization was given in units of $\frac{\mu_B}{\text{molecule}}$ we make a quantitative comparison with our calculation. We get from ref.[9] for $B = 15\text{T}$ an experimental value of $\approx 41.5 \frac{\mu_B}{\text{molecule}}$ for 2 TGG molecules and from our calculation $|\langle \vec{J} \rangle|_{[110]} = 4.72/(\text{Tb ion})$. This gives for 6 Tb ions and $g_L = 1.5$ a value of $42.5 \frac{\mu_B}{2\text{molecules}}$ in close agreement with the experiment of ref.[9].

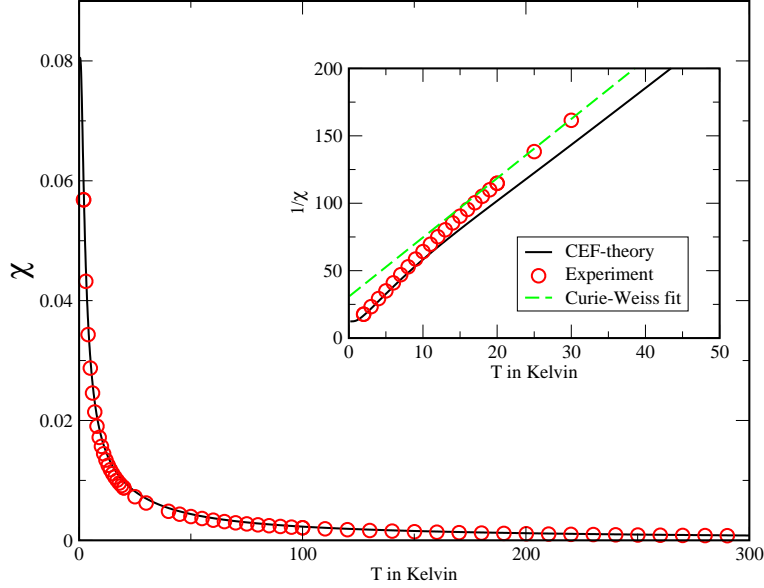


FIG. 3: Measured magnetic susceptibility χ (red points) and result of CEF-calculation (black line) versus temperature in Kelvin. The inset shows the same data plotted as $1/\chi$ compared with a Curie-Weiss fit (green dashed line). All the susceptibilities shown are dimensionless.

IV. MAGNETIC SUSCEPTIBILITY

The magnetic susceptibility was measured in the temperature range between $2\text{K} \leq T \leq 300\text{K}$ and in a magnetic field of $B = 0.1\text{T}$ using a Quantum Design SQUID magnetometer. All measurements were performed on a single crystal with the external field oriented parallel to the cubic $[100]$ direction. The data were corrected for the temperature-independent diamagnetic core contribution and the magnetic contribution of the sample holder. The latter was determined from an independent measurement. The experimental data versus temperature are shown in fig.3.

A fit by a Curie-Weiss law $\chi^{-1} = (T - \Theta)/C$ from 10K to 300K gives $\Theta = -7\text{K}$ and the Curie constant $C = 0.2277\text{K}$. Evaluating C gives an effective magnetic moment of $p_{\text{eff}} = 9.25$ close to $p_{\text{eff}} = g_L \sqrt{J(J+1)} = 9.72$ for $J = 6$ at high temperatures. A $\theta = -7\text{K}$ compared with a Néel-temperature $T_N = 0.35\text{K}$ implies a strongly frustrated spin system in the ordered anti-ferromagnetic region.

We also calculated the magnetic susceptibility of TGG using the CEF scheme, that is we calculated $\chi^i(T)$ of ion i in the laboratory system from the free energy with the formula

Density	$\rho = 7.22 \text{ g/cm}^3$
Molecular weight	$M = 1017.37$
Molvolume	$V_M = 140.91 \text{ cm}^3/\text{Mol}$
Number of Tb-ions per cm^3	$n = 1.28 \times 10^{22} \text{ cm}^{-3}$
Landé g-factor	$g_L = 1.5$

TABLE III: Physical parameters for TGG

$$\begin{aligned}
\chi^i(T) = -\frac{\partial^2 F^i}{\partial B_z^2} = & \frac{1}{Z^2} \frac{1}{k_B T} \left(\sum_n \langle n | J_z | n \rangle \exp\left(\frac{-E_n}{k_B T}\right) \right)^2 \\
& - \frac{1}{Z} \frac{1}{k_B T} \sum_n |\langle n | J_z | n \rangle|^2 \exp\left(\frac{-E_n}{k_B T}\right) \\
& + \frac{2}{Z} \sum_{n \neq m} \frac{|\langle n | J_z | m \rangle|^2}{E_n - E_m} \exp\left(\frac{-E_n}{k_B T}\right) \quad \text{with } i = 1, \dots, 6
\end{aligned} \quad (3)$$

and obtained the total susceptibility $\chi(T) = \sum_{i=1}^6 \chi^i(T)$ by summing over the contributions from the six inequivalent ions. It is obvious that the magnetic susceptibility of cubic TGG is isotropic. This can be also seen from fig.2 where the initial slopes for the 3 different field directions are the same. The calculated susceptibility is plotted as a function of temperature together with the experimental data in fig.3 . The measured χ_m in cm^3/Mol TGG has been divided by the molvolume using the parameters of table III. Without any fitting parameters the agreement between experiment and calculation can be considered as very good, except for a small deviation between 20K and 50K.

As an example we compare the calculation with the experiment for $T = 20\text{K}$. From eq.3 we get that $\frac{d\langle J_i \rangle}{dB} = 0.548 T^{-1}$ at $T = 20\text{K}$. With $M_i = n g_L \mu_B \langle J_i \rangle$ and the values of table III this leads to $\chi_m = 0.97 \times 10^{-2} \text{ cm}^3/\text{cm}^3$ which has to be compared with the experimental value $\chi_{\text{exp}} = 0.88 \times 10^{-2} \text{ cm}^3/\text{cm}^3$.

V. ESR EXPERIMENTS

The ESR experiments were done employing a multiple-frequency 14 T ESR spectrometer [15] equipped with a millimeter-wave vector network analyzer (product of AB Millimetre) and a 16 T ESR spectrometer equipped with VDI radiation sources (product of Virginia Diodes Inc.) similar to that described in [16]. The external field was applied parallel to the

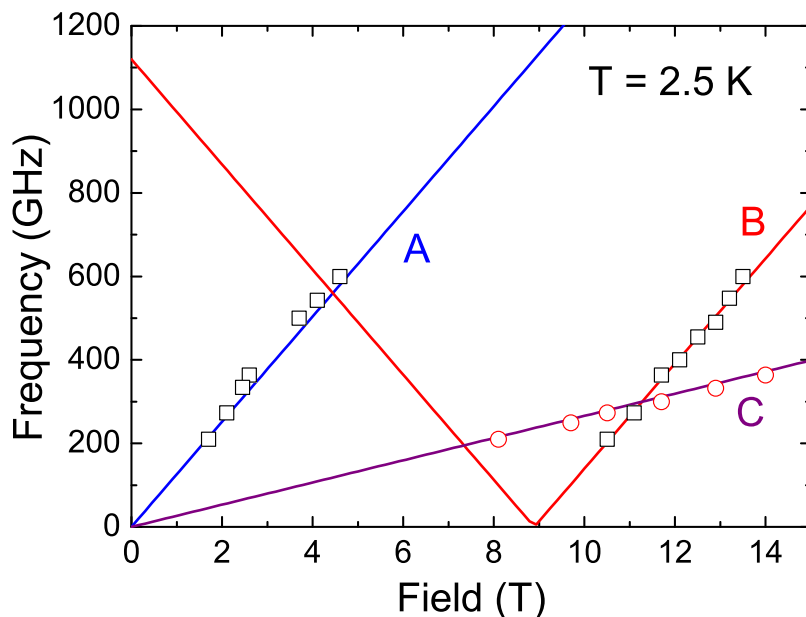


FIG. 4: ESR transitions measured at $T=2.5\text{K}$, with the field parallel to the $[110]_c$ direction. The lines correspond to ESR modes as described in the text.

propagation direction of the electromagnetic radiation and with perpendicular incidence on the $[110]_c$ face of the TGG crystal. The electromagnetic field vectors \vec{e}, \vec{b} are in free space transverse waves and the Zeeman Hamiltonian reads

$$H_z = g\mu_B \vec{J} \vec{b}_{rf} \quad (4)$$

with linear polarized waves and propagation direction $\vec{k} \parallel [110]_c$, which in the local coordinate systems corresponds to the z-direction and the $(\sqrt{\frac{1}{2}}, \pm\frac{1}{2}, \frac{1}{2})$ directions respectively. We performed the measurements in the frequency range 200-600 GHz.

Experimentally we found 3 ESR lines, labelled A, B and C. Fig.4 shows the resonances we found at 2.5K and fig.5 gives the temperature dependence of the resonance lines up to 97 K. Trying to identify these lines within our calculated level scheme (fig.1 a,b,c) we find that there are only few transitions which we can expect to be detectable and which we actually have observed in ESR.

To ensure that the transitions we consider have nonvanishing weight we also calculated

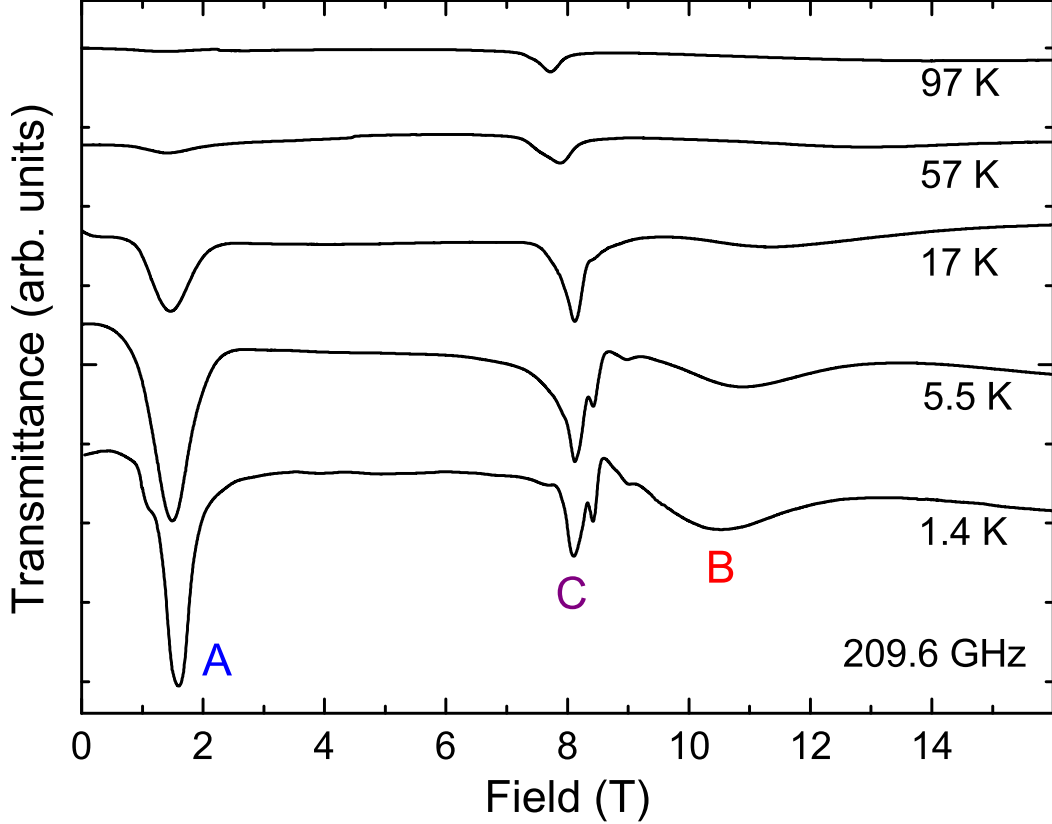


FIG. 5: Temperature dependence of the three observed ESR-lines A,B,C at a frequency of 209.6 GHz. The field is applied in $[110]_c$ direction. Note, that the ESR spectra are offset for clarity.

the ESR transition matrix elements $\langle m|J_x|n\rangle$ and $\langle m|J_y|n\rangle$ between levels n,m . The relevant transition probabilities are shown in the fig. 6. Since however the microwave intensities used in the experiment are strongly dependent on the frequency we can only make a qualitative comparison with the calculated matrix elements.

In detail we considered the following transitions in the level scheme as possible candidates for the experimentally observed lines A,B and C: For the ions of type 1 (fig 1a) and magnetic field below 9 Tesla the transition from the quasidegenerate doublet to the second state has nonvanishing matrix elements (fig 6 d) (note that we count the ground state as line 0, line 1 represents the first excited state, etc). Also transitions from excited states i.e. between line 2 and line 3 or line 4 have nonvanishing weight (see figure 6 a and b). For ions of type 1 and magnetic field larger than 9 Tesla we expect that the transition between the ground state and line 1 or 2 should be detectable (fig. 6c), however the transition (0-2) has vanishing weight in this field range (fig. 6d).

For the ions of type 2,3,5,6 (fig 1b) there are two possible ESR-transitions: For magnetic field below 9 Tesla the transition $0 \leftrightarrow 1$ (see fig. 6e) and the transition $1 \leftrightarrow 2$ (see fig.6f).

For ions of type 4 (fig 1c) we do not expect to see any transitions in ESR.

Next comparing the calculated level scheme with the experimental results shown in fig. 4 we come to the following conclusion:

Line A: From the frequency and temperature dependence we can conclude that we deal here with a transition from the ground state. It is an increasing branch and can be observed in the field region between 1.7 to 4.7 Tesla (see fig.4). It can be nicely fitted within the levels 0-1 for ions 2,3,5,6 (fig.1 and fig.6) and gives, using $h\nu = g\mu_B B$ a g-factor 9.34 from the level scheme and from experiment we find a g-factor of $g = 9$. Above 9T one cannot follow this line further because the corresponding energy levels (0-1) are constant and the matrix elements are vanishing.

Line B: Also line B is a ground state excitation between the energy levels 0-1 and 0-2 for ion 1 (fig.1 a) but observed in experiment only for $B > 10.5T$. Also the corresponding matrix element $\langle 0|J_{x,y}|1\rangle$ is vanishing below 9T (fig.6) which thus corresponds to our experimental finding. Note that matrix element $\langle 0|J_y|2\rangle$ has some weight for magnetic field close to 9T on both sides. Since this is a decreasing branch we could observe such a transition only below 7.4T with our lowest microwave frequency of 200 GHz. But for these fields the matrix element becomes rather small. Therefore line B can only be observed for $B > 9T$. The experiment gives data up to 14T despite the fact that the corresponding matrix elements become rather small. This can be due to the fact that the microwave intensity is rather large for the higher frequencies as mentioned above. The g factor for the observed B-line is again $g = 9$ and from our calculation we find $g=8.7$.

Line C: Finally the observed line C has spectral weight above and below the level transition of 9T as seen in fig.4. It has a g factor of $g = 1.9$ and cannot be fitted easily into the level scheme of fig.1. Since it is visible already at low temperatures we conclude that it cannot be a transition within excited states, in particular it cannot be identified with the transition 1-2 for ions of type 2,3,5,6 which has a g-factor $g=1.6$.

But there are other possibilities for line C. One obvious idea is a resonance line due Tb^{4+} impurities. It is known that the garnet structure can have Tb^{4+} with $L = 0$, $S = J = \frac{7}{2}$ like Gd^{3+} . This could give a line with $g = 2$ as observed. By tilting the sample in the magnetic field by 10° and 20° respectively the line splitted up considerably for the frequency $\nu = 96.8$

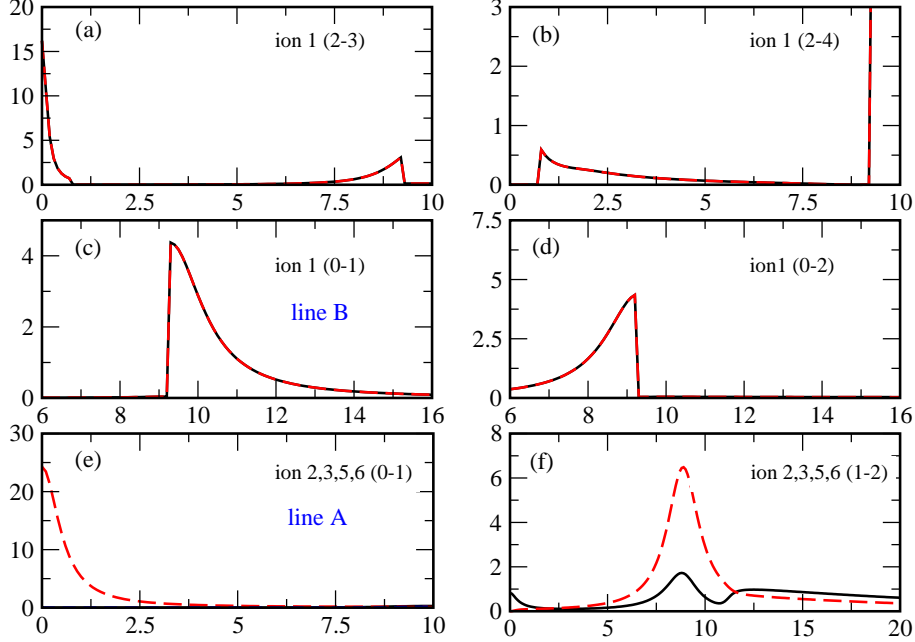


FIG. 6: Calculated ESR transitions matrix elements $|\langle m|J_i|n\rangle|^2$, Where $i=x$ is depicted as black line and $i=y$ as red dashed line. The abscissa is always the magnetic field in Tesla.

GHz. This should not occur for a S-state ion with complete isotropy. But a splitting occurs for line A too. Another possibility is a Tb^{3+} ion on octahedral site substituting a Ga^{3+} ion (see ref.[5]).

Considering the energy level diagram for the six different Tb^{3+} ions and the given frequency range at our disposal the following points should be noted: We cannot observe the splitting of the quasi doublet with $\Delta E = 3.7K = 77GHz$. We have not observed other transitions from excited states although we took measurements up to temperatures of 100K. The observed resonances are all on branches with increasing field.

To summarize, we find that the two ESR-lines A and B shown in fig.4 correspond very well with our calculations. The effective g-factor is $g = 9.34$ for resonance A for $B < 9T$ and ions 2,3,5,6. For resonance B and $B > 9T$ we find an effective g-factor $g = 8.7$ for ion 1. as compared to the experimental value of $g = 9$ for both line A and line B.

We want to emphasize here, that the description by the model given in Eq. 1 is of course limited. Also the crystal-field parameters, which are usually determined at low magnetic fields might be slightly field dependent and it is not clear to what extend the small but nonzero exchange interaction modifies the energy levels.

f_{20}	f_{22}	f_{40}	f_{42}	f_{44}	f_{60}	f_{62}	f_{64}	f_{66}
2	$\frac{2}{\sqrt{6}}$	8	$\frac{8}{\sqrt{40}}$	$\frac{8}{\sqrt{70}}$	16	$\frac{16}{\sqrt{105}}$	$\frac{16}{\sqrt{126}}$	$\frac{16}{\sqrt{231}}$

TABLE IV: Coefficients f_{ij}

VI. SUMMARY

Taking all the presented experiments together we can say that the CEF scheme, introduced by Guillot et al [9], can explain magnetization, magnetic susceptibility and ESR lines quite well. It is rather satisfying that all these widely different magnetic effects presented in this paper originate in a complicated garnet structure with 6 Tb ions with different local symmetries, which can be quantitatively described. In the discussions for the magnetization M, the magnetic susceptibility χ and the ESR we have neglected interaction effects between the ions. The existence of T_N and Θ point of course to interaction effects. But they are too small to be observed in the magnetization M and in ESR.

VII. APPENDIX

The B_{ij} used in eq.1 can be calculated from the b_{ij} given in table I by the following equations:

$$\begin{aligned}
B_{2j} &= \frac{b_{2j}\alpha_J}{f_{2j}} & j = 0, 2 & \quad (5) \\
B_{4j} &= \frac{b_{4j}\beta_J}{f_{4j}} & j = 0, 2, 4 & \\
B_{6j} &= \frac{b_{6j}\gamma_J}{f_{6j}} & j = 0, 2, 4, 6, &
\end{aligned}$$

where

$$\alpha_J = \frac{-1}{99} \quad (6)$$

$$\beta_J = \frac{2}{16335} \quad (7)$$

$$\gamma_J = \frac{-1}{891891} \quad (8)$$

and the f_{ij} are listed in table IV.

Acknowledgments

This work was partly supported by the Deutsche Forschungsgemeinschaft and EuroMagNET II (EU contract No. 228043).

- [1] K. Kamazawa, Despina Louca, R. Morinaga, T.J. Sato, Q. Huang, J.R.D. Copley and Y. Qiu, *Phys.Rev.B* **78**, 064412 (2008).
- [2] J. Hammann and P. Manneville, *J. de Phys.* **34**, 615 (1973).
- [3] A.P. Ramirez, in *Handbook on Magnetic Materials*, edited by K.J.H. Buschow (Elsevier, Amsterdam, 2001), Vol. 13,p 423.
- [4] C. Strohm, G.L.J.A. Rikken and P. Wyder, *Phys. Rev. Lett.* **95**, 155901 (2005).
- [5] A.V. Inyushin and A.N. Taldenkov, *JETP Letters* **86**, 379 (2007); *JETP* **111**, 760 (2010).
- [6] A. Sytcheva, U. Löw, S. Yasin, J. Wosnitza, S. Zherlitsyn, T. Goto, P. Wyder, and B. Lüthi, *J.Low Temp. Phys.* **159**, 126 (2010).
- [7] A. Sytcheva, U. Löw, S. Yasin, J. Wosnitza, S. Zherlitsyn, P. Thalmeier, T. Goto, P. Wyder, and B. Lüthi, *Phys. Rev. B* **81**, 214415 (2010).
- [8] K. Araki, T. Goto, Y. Nemoto and B. Lüthi., *Eur. Phys. J. B* **61**, 257 (2008).
- [9] M. Guillot, A. Marchand, V.Nekvasil and F. Tcheou, *J.Phys. C* **18**, 3547 (1985).
- [10] M. T. Hutchings, *Solid State Phys.* **16**, 227-273 (1964).
- [11] B. G. Wybourne, *Spectroscopic Properties of Rare Earths* (J. Wiley and Sons, Inc., New York, 1965).
- [12] R.Z. Levitin, A.K. Zvezdin, M.von Ortenberg, V.V. Platonov, V.I. Plis, A.I. Popov, N. Puhlmann, and O.M. Tatsenko, *Physics of the Solid State*, Vol 44, No.11, 2107 (2002).
- [13] A.R. Edmonds, *Angular Momentum in Quantum Mechanics*, *Princeton Landmarks in Physics*, (Princeton University Press 1974).
- [14] P.A. Lindgård, O. Danielsen, *J.Phys. C* **7**, 1523 (1974).
- [15] C. Golze, A Alfonsov, R. Klingeler, B. Büchner, V. Kataev, C. Mennerich, H.-H. Klauss, M. Goiran, J.-M. Broto, H. Rakoto, S. Demeshko, G. Leibelng, and F. Meyer, *Phys. Rev. B* **73**, 224403 (2006).
- [16] S.A. Zvyagin, J. Krzystek, P.H.M. van Loosdrecht, G. Dhahlenne, A. Revcolevschi, *Physica B*

346, 1 (2004).